

Role of Organic and Inorganic Additives on the Assembly of CTAB-P123 and the Morphology of Mesoporous Silica Particles

Altug S. Poyraz and Ömer Dag*

Department of Chemistry, Bilkent University, 06800, Ankara, Turkey

Received: July 30, 2009; Revised Manuscript Received: September 16, 2009

Mesoporous silica particles with various morphologies and structures have been synthesized by controlling the solubility, micellization, and assembly of a charged surfactant (cetyltrimethylammonium bromide, CTAB) and a pluronic (PEO₂₀PPO₇₀PEO₂₀, P123) couple using an organic (benzene) or an inorganic (SO₄²⁻, NO₃⁻, or Cl⁻) additive. The effect of CTAB, with or without one of the Hofmeister ions or benzene in various concentrations, on the morphology, pore-size, pore-structure and the nature of the silica particles has been investigated. Increasing the lyotropic anion (SO₄²⁻) or benzene concentration of the synthesis media creates wormlike particles with enlarged pores and reduced wall thickness. However, the hydrotropic anion (NO₃⁻) influenced the solubility of the charged surfactant and increased the CTAB concentration in the CTAB-P123 micelles, and as a result, in the mesoporous silica particles. The surface area, unit cell, and pore size of the silica particles are diminished by increasing the nitrate ion concentration. The effects of the Cl⁻ ion are between the SO₄²⁻ and NO₃⁻ ions. It influenced the P123 at low and CTAB at high concentrations. At low CTAB/P123 mol ratios, the Cl⁻ ion affects mainly the P123, but at high CTAB/P123 it affects both the CTAB and P123. By carefully adjusting these ingredients (CTAB, SO₄²⁻, Cl⁻, NO₃⁻ and benzene), not only the morphology of the particles, but also the pore-size and pore-structure of the mesoporous silica particles could be adjusted. The investigations were carried out by preparing a series of powder samples and, by varying the CTAB/P123 mol ratio (between 3.0 and 6.0) and the concentration of the organic (0.17 to 0.90 M) or inorganic (at 0.25, 0.50, or 1.00 M) additive in the synthesis media. The powder samples were analyzed using microscopy (SEM, TEM, and POM), diffraction (PXRD), and spectroscopy (FTIR, Raman, UV-vis, and EDS) techniques toward above goals.

Introduction

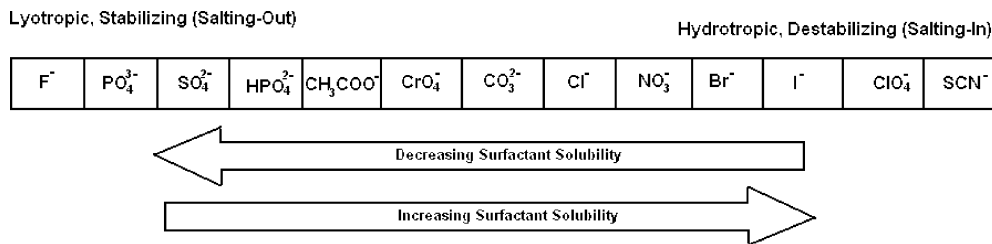
Since the first synthesis of mesoporous silica,^{1,2} there has been tremendous amount of effort dedicated to modifying these materials during the synthesis using additives or by using chemical treatments after the synthesis. As of yet, there are no systematic studies investigating the role of these additives at the molecular level. Ozin et al. investigated for the first time various shapes in powder samples obtained from an acidic solution of CTAB and a silica source.³ Since then, the ordered mesoporous silica particles have been synthesized in various morphologies, such as spheres,^{4–6} crystal-like,^{5–8} wormlike,^{3,6,9,10} hollow spheres,¹¹ gyroid,^{8,9} and toroids etc.^{8,12} The morphology, monodispersity, pore size and pore structure are some of the key parameters that need to be addressed for many applications, such as drug delivery systems, photonic crystals, chromatography, and catalysis.^{4,10,13–16}

The pluronic surfactants are commonly used in many investigations because of their nontoxic, cheap and excellent aggregation properties.^{17–19} These surfactants are triblock copolymers with a relatively hydrophobic group, poly(propylene oxide) (PPO), at the middle and relatively hydrophilic, poly(ethylene oxide) (PEO), head groups at both ends of the polymer (PEO_x–PPO_y–PEO_x). One of the characteristics of the mesoporous materials synthesized using the pluronic type surfactants is their thick walls that are typically around 3.0–7.0 nm.^{20–22}

Alkali metal salts have been used to investigate the effects of anions from the Hofmeister's series in the aqueous surfactant solution and also on the synthesis of the mesoporous silica.^{6,7,23–25} Li et al.²⁰ investigated the role of KCl on the pore structure of the mesoporous silica particles. Zhao et al.^{7,22} observed a remarkable impact of KCl and K₂SO₄ on both the morphology and mesostructure of the silica particles. In addition to the pore structure and morphology, the salt ions also affect the wall thickness by adjusting the hydration of the PEO units in the corona region of the micelles.²⁶ The ultimate effect of the organic and inorganic additives is to change the hydrophilic–hydrophobic character of the pluronic micelles. For instance, the aggregation behavior of a more hydrophobic surfactant can be simulated by decreasing the solubility of a pluronic with the additives or by increasing the temperature of the media.^{17,27–30}

A temperature increase in the media decreases the surfactant solubility and puts force on the surfactants for more effective packing. Therefore, the number of surfactants inside the micelle increases in order to pack itself more effectively.^{30–32} A similar impact could also be created by using the salts of the Hofmeister's series.^{18,20,33,34} These salts can be collected into two main groups. The ones on the left-hand side, called lyotropic anions, decrease solubility and enhance aggregation; however the ones on the right-hand side, the hydrotropic anions, enhance the hydrophilicity and the solubility of the pluronics in an aqueous media.^{25,35} The lyotropic ions decrease the critical micelle concentration (cmc), critical micelle temperature, and the cloud point of the pluronics. The strength of this effect depends on the type and concentration of the anion.^{17,18,23,24,32,34–37} Moreover,

* To whom correspondence should be addressed. Phone: 90-312-2903918. Fax: 90-312-2664068. E-mail: dag@fen.bilkent.edu.tr.



it has also been shown that the usage of these lyotropic anions influences the type of aggregation and shape of the micelles.²³

The commonly used organic additives are trimethyl benzene, benzene, butanol, alkanes, and cyclohexane. The main goal of the additives is to change the morphology and to tune the pore size^{26,38–43} by means of changing the micellization properties of the pluronics.^{43–45} Moreover, once the organic additives penetrate the micelles they increase the hydrophobic character and the micelles swell.^{39–43} Increasing the hydrophobic character of the micelles results in a change in the geometry of the mesoporous silica particles from spherical to wormlike.⁶ Nagarjan et al. investigated the solubilization capacity of organic molecules in the pluronic micelle core and suggested that benzene is the best nonpolar solute.^{44,45} The nonpolar solvents are widely employed in the synthesis of mesoporous silica materials to enlarge the pores. The pore swelling agents also increase the structural order of the silica particles.^{26,40–42}

In this investigation, we have employed two surfactants, namely CTAB and P123, and controlled the hydrophilic–hydrophobic balance in the coupled micelles, CTAB-P123, by the CTAB and additive (Na_2SO_4 , $NaNO_3$, KCl , or benzene) concentrations to control the morphology, pore size, and pore structure of the silica particles. The investigation was carried by analyzing the samples by means of diffraction, microscopy, and spectroscopy techniques.

Experimental Part

Synthesis of Mesoporous Silica Particles. The P123 ($PEO_{20}PPO_{70}PEO_{20}$, MW = 5750 g/mol) and CTAB (with a CTAB/P123 mol ratios between 0 and 12) were dissolved by stirring in a 0.1 M 100 mL aqueous HCl solution. To the above clear solution, 2.5 mL (1.64×10^{-2} mol) tetramethylorthosilicate (TMOS) was added under vigorous stirring at RT. The resulting clear solution was put directly into plastic bottles, which were kept in a 95 °C oven for five days. Then, the precipitate was filtered and washed three times with 50 mL portions of distilled water and then dried in a 60 °C oven for three days. The dried samples were calcined with rapid calcination method in air at 600 °C for 4 h.⁴⁶ In a typical synthesis, the mole ratios of the chemicals used are 1:4:56:21735:65 corresponding to P123/CTAB/HCl/H₂O/TMOS. The same procedure has also been employed in the presence of different alkali salts (KCl , Na_2SO_4 , and $NaNO_3$) over a wide concentration range (between 0.2 and 1.0 M) and benzene between 0.17 and 0.90 M. All the additives were added and dissolved completely just before addition of the silica source, TMOS.

Characterizations. The powder X-ray diffraction (PXRD) patterns were collected using a Rigaku Miniflex diffractometer using a high power Cu K α source operating at 30 kV/15 mA. The PXRD patterns of both the as-synthesized and calcined powder samples are packed on metal powder holders and collected in 0.9–8.0 (2θ) range with a 1.0°/minute scan rate. Fourier Transform Infrared (FT-IR) spectra were collected using Bruker Tensor 27 model FTIR spectrometer, that uses a

DigiTect™ DLATGS detector. The resolution of the measurements were 4 cm^{-1} and 128 scans were collected in absorbance mode for each powder sample in the 400–4000 cm^{-1} range. The samples were prepared as KBr pellets. The micro-Raman spectra were recorded on a LabRam model confocal Raman microscope with a 300 mm focal length. The spectrometer was equipped with a MPC 6000 DPSS laser power supply with a 532.1 nm green laser. The signal collected was transmitted through a fiber optic cable into a spectrometer with a 600 groove/mm grating. The spectra were collected by placing and flattening powder samples on microscope slides and manually placing the probe tip near the desired point on the powder sample. The UV–vis absorption spectra were recorded using a Varian Carry 5 double-beam spectrophotometer to determine the micellization studies using ethylene orange as an indicator. The scanning electron microscope (SEM) images were recorded using ZEISS EVO-40. The samples were prepared on aluminum sample holders by carefully dispersing powder samples with the help of acetone. The images were recorded at 15 kV (EHT) operating voltage and at around 1.900A filament current. The EDS data were collected on the SEM using a Bruker AXS Xflash detector 4010. The transmittance electron microscope (TEM) images were recorded on a FEI Technai G2 F30 at an operating voltage of 200 kV. The calcined powder samples were ground in a mortar, then dispersed in 5 mL of acetone using sonicator for 5 min. One drop of the dispersed acetone solution was put on a TEM grid and dried on hot-plate. The N_2 (77.4 K) sorption measurements were performed with a TriStar 3000 automated gas adsorption analyzer (Micrometrics) in a relative pressure range, P/P_0 , from 0.01 to 0.99. To provide high accuracy and precision in the determination of P/P_0 , the saturation pressure P_0 was measured in 120 min intervals. The powder samples were dehydrated under ($\sim 10^{-2}$ torr) vacuum for 4 h at 400 °C before the measurements in order to remove adsorbed water and volatile species in the pores.

Results and Discussion

The Synthesis of Mesoporous Silica Particles. Both the organic and inorganic additives have a significant impact on the assembly properties of the P123 and CTAB surfactants. Influencing their micellization also affects the meso-order in the mesoporous silica particles. The effect of CTAB on the morphology of the mesoporous silica has been outlined before⁶ and it was found that at a CTAB/P123 mol ratio of 3.0, the particles are a mixture of spherical and wormlike. Further increasing CTAB/P123 mol ratio in the reaction media produces only spherical particles but the excess CTAB produce film samples at the air water interface.⁶ In this investigation, we consider 3.0 CTAB/P123 mol ratio as the low and 6.0 as the high in the presence of another additive, such as the salts and benzene.

To demonstrate the effect of the Hofmeister anions, we also performed a set of dye experiments in which ethylene orange (EO, an acid–base indicator) was used as a micelle indicator

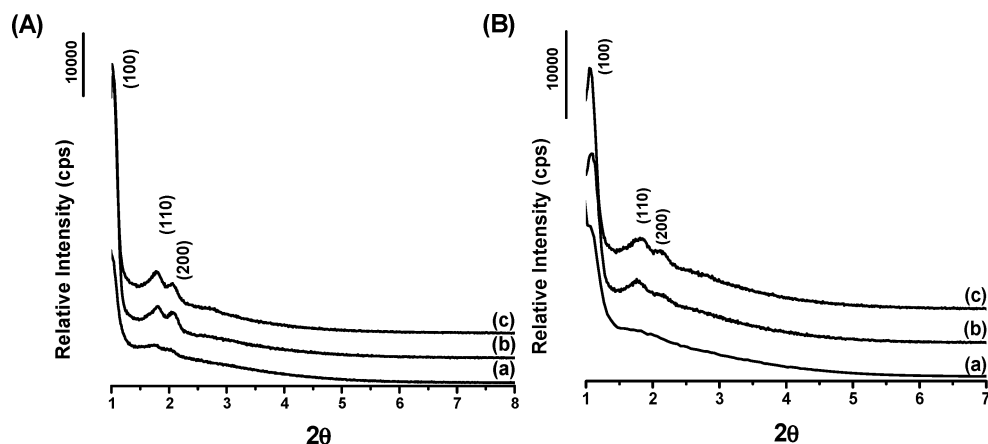


Figure 1. The PXRD patterns of the mesostructured silica obtained from the CTAB–P123– SO_4^{2-} system using (A) CTAB/P123 mol ratio of 3.0 and sulfate concentration of (a) 0.0, (b) 0.25, (c) 0.5 M and (B) CTAB/P123 mol ratio of 6.0 and sulfate concentration of (a) 0.0, (b) 0.25, and (c) 0.5.

in the formation of micelles in an aqueous media (similar to our synthesis conditions). The EO molecules prefer the core of the micelle and its color change from orange to yellow where the absorption peak in the visible region of the spectrum shifts to higher energy (see Supporting Information Figure S1A,B). We have used this behavior of the EO to investigate the micellization using UV–vis absorption spectroscopy techniques. Because of some limitations of the EO molecules (it only responds to micellization under neutral conditions) and the micellization behavior of P123 (the P123 molecules are always micellar at even much lower concentrations), this investigation has been limited to P85 ($\text{PEO}_{38}\text{PPO}_{43}\text{PEO}_{38}$), pH 5.5 (neutral), and various salt concentrations to investigate the effect of specifically the inorganic additives. Supporting Information Figure S1C shows the micellization behavior of P85 in the presence of each the following salts at 0.5 M concentrations: NaF, Na_2SO_4 , KCl, NaNO_3 , KI, and KSCN. The trend in the figure clearly shows that the lyotropic anions enhance the micellization, whereas the hydrotropic anions have an opposite effect (see Supporting Information).

The sulfate ion enhances the micellization and decreases the solubility of P123 at lower concentrations. Therefore, the SO_4^{2-} ions were used at 0.0, 0.25, and 0.50 M, relatively lower concentrations than the NO_3^- and Cl^- ions (used at 0.0, 0.50, and 1.00 M concentrations). The nitrate ion, NO_3^- has almost no effect on the micellization of P123, but it affects the assembly properties of CTAB by interacting with the positively charged headgroup. A third anion (Cl^-) has been used, where its effect is between the sulfate and nitrate ions. The chloride ion affects both P123 and CTAB. Its effect is similar to a combination of sulfate and nitrate ions. The benzene molecule was used as an organic additive, specifically between 0.17 and 0.90 M concentrations. The benzene molecule diffuses into the core of the micelles, dehydrates the core and core–corona interface and swells the micelles, and as a result increases the pore size of mesoporous materials. Moreover, it also enhances the meso-order in the mesoporous silica particles. All concentrations of the additives were optimized based on their effect on the morphology of the silica particles.

The Effect of Sulfate Ion in the CTAB–P123– SO_4^{2-} Synthesis System. The sulfate ions decrease the solubility, increase the aggregation number, and change the geometry of the CTAB–P123 micelles. The presence of a sulfate ion in the synthesis media creates (i) more densely packed micelles, (ii) a dehydrated core in the micelle, (iii) enhanced hydrophobic

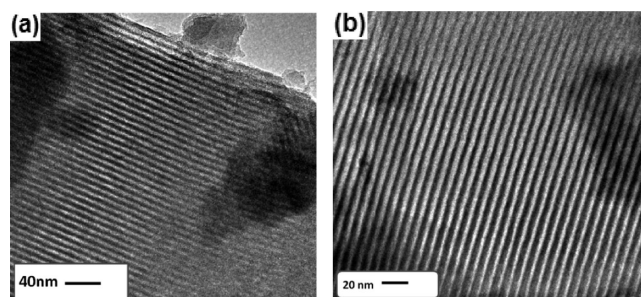


Figure 2. The TEM images of the mesostructured silica particles obtained from the CTAB–P123– SO_4^{2-} system, SO_4^{2-} ion concentration is 0.5 M and the CTAB/P123 mol ratios of (a) 4.0 and (b) 6.0.

interactions, and (iv) better ordered mesoporous materials. Figure 1 shows the PXRD patterns of the mesoporous silica particles, synthesized at two different SO_4^{2-} ion concentrations and two different CTAB/P123 mol ratios. In the absence of SO_4^{2-} ion, the PXRD of the silica particles displays one sharp diffraction line due to the (100) plane and relatively broad and overlapped (110) and (200) lines of the 2D hexagonal mesostructure. At low CTAB/P123 mol ratios (3.0 and 4.0) and 0.25 M SO_4^{2-} ions, besides the very high diffraction intensity of the (100) plane, the other diffraction lines (110) and (200) are also better resolved; see Figure 1. Moreover, in the presence a 0.5 M SO_4^{2-} concentration, diffraction lines originating from (210) and (300) planes are also observed, Figure 1. All diffraction lines can be indexed to a well ordered 2D hexagonal mesostructure with a unit cell parameter a of 10.2 nm. At a high CTAB/P123 mol ratio (6.0), the three diffraction lines ((100), (110) and (200)) are still well resolved, but they are broader and have lower intensity and are shifted slightly to higher angles when compared to the diffraction lines obtained from the particles synthesized at lower CTAB/P123 mol ratios. The unit cell parameter a (9.4 nm) is slightly smaller at a high CTAB/P123 ratio. The TEM images, shown in Figure 2, also correlate to the structure being well ordered. A long-range order in a meso scale can be clearly seen in these images. The spacing between the lines is around 7.8 nm at the lowest and 7.2 nm at the highest CTAB/P123 mol ratio, which is also consistent with the shift in the PXRD patterns.

The stronger hydrophobic interactions in the core of the micelles cause a better ordered pore structure and also influence the morphology of the silica particles. Figure 3 shows the SEM images of the particles, obtained from the CTAB–P123– SO_4^{2-} system, at different CTAB/P123 mol ratios and SO_4^{2-} ion

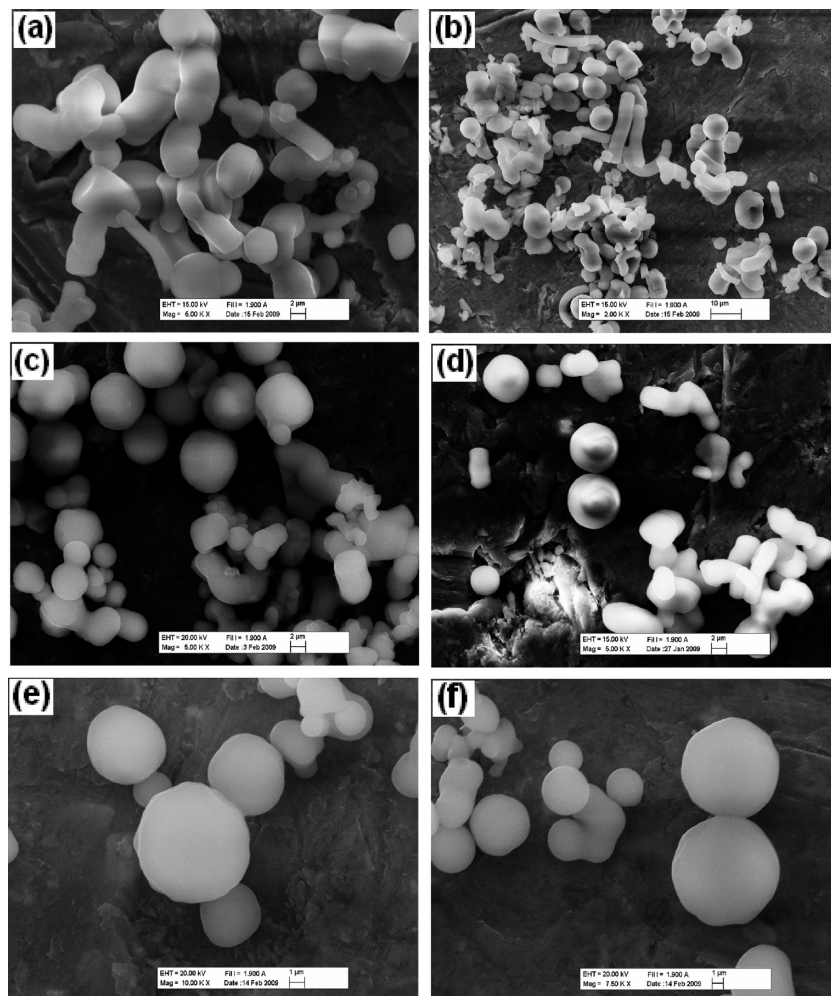


Figure 3. The SEM images of the samples obtained from the CTAB–P123–SO₄²⁻ system; for the CTAB/P123 mol ratio of 3.0 and the SO₄²⁻ concentration of (a) 0.25 and (b) 0.5 M, the CTAB/P123 mol ratio of 4.0 and the SO₄²⁻ concentration of (c) 0.25 and (d) 0.5 M, and the CTAB/P123 mol ratio of 6.0 and the SO₄²⁻ concentration of (e) 0.25 and (f) 0.5 M.

TABLE 1: The Structural Parameters of the Mesoporous Silica Particles, Obtained from the CTAB–P123–SO₄²⁻ System with Different CTAB/P123 Mol Ratios and SO₄²⁻ Concentrations

CTAB/P123 mol ratio	Na ₂ SO ₄ concentration (M)	BET surface area (m ² /g)	<i>d</i> ₁₀₀ (nm)	pore size ^a 2 <i>r</i> (nm)	wall thickness ^b (nm)	pore volume (cm ³ /g)
3	0	690	8.8	5.9	4.3	0.40
	0.25	684	8.6	6.9	3.0	0.96
	0.5	630	8.7	6.6	3.4	0.75
4	0	685	7.9	4.1	5.0	0.34
	0.25	528	9.3	5.7	5.0	0.84
	0.50	672	8.2	7.0	2.5	0.84
6	0	723	8.4	4.6	4.7	0.54
	0.25	674	8.1	5.5	3.8	0.65
	0.50	644	8.3	6.0	3.6	0.71

^a Pore diameter is calculated from the adsorption branch of the isotherm using BJH method. ^b The wall thickness (*t*) is obtained by deducing the pore diameter (2*r*) from the unit cell *a*₀ (*a*₀ = (2/√3)*d*₁₀₀), namely, *t* = *a*₀ – 2*r*.

concentrations. Also note that the particles, synthesized using CTAB/P123 mol ratio of 3.0 (no sulfate), are mainly spherical (with a small amount of wormlike particles); at a mole ratio above 3.0 CTAB/P123, all particles are spherical. The addition of the Na₂SO₄ salt increased the number of wormlike particles.

The further increase to 0.5 M SO₄²⁻ ion in the synthesis media resulted in only wormlike particles. At higher CTAB concentrations (CTAB/P123 mol ratio of 6.0), the particles are spherical (with cornered surfaces rather than smooth surfaces). Our observations suggest that increasing the CTAB in the media

favors the spherical particles, but increasing SO₄²⁻ ion concentration enhances the formation of wormlike particles. The presence of a high concentration of both CTAB and sulfate forces the formation of crystal-like particles. Much higher SO₄²⁻ ion concentrations were also tested (1 and 2 M), where it is not possible to dissolve P123. It is known that the lyotropic anions, especially the sulfate ion, sharply decrease the cmc of the pluronic surfactants. Also note that the solution is cloudy in the presence of 0.25 and 0.50 M SO₄²⁻ ions, indicating that the P123 molecules aggregate into much larger particles. However,

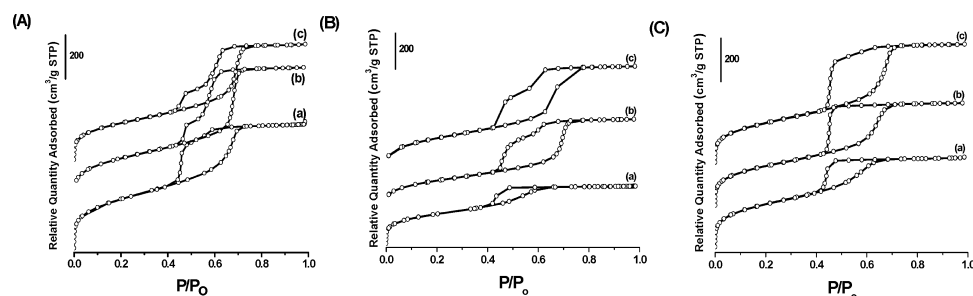
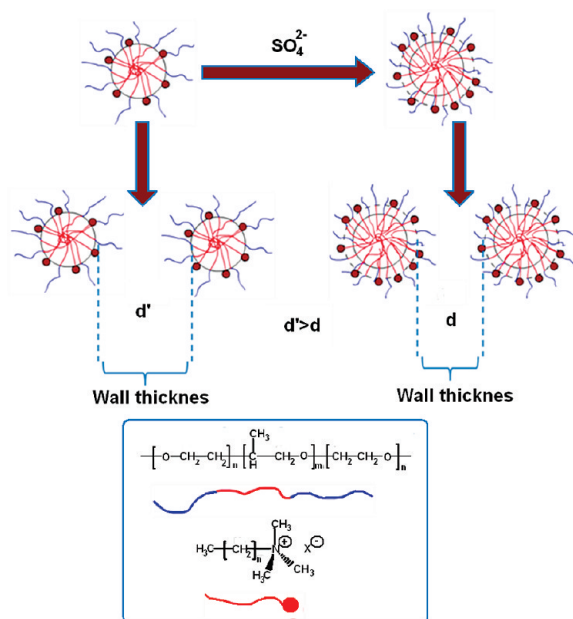


Figure 4. The N_2 adsorption–desorption isotherms at 77 K of the mesoporous silica particles obtained from the CTAB–P123– SO_4^{2-} system. (A) For the CTAB/P123 mol ratio of 3.0, the SO_4^{2-} ion concentration of (a) 0.0, (b) 0.25, and (c) 0.5 M, (B) for the CTAB/P123 mol ratio of 4.0, the SO_4^{2-} ion concentration of (a) 0.0, (b) 0.25, and (c) 0.5 M, and (C) for the CTAB/P123 mol ratio of 6.0 and the SO_4^{2-} ion concentration of (a) 0.0, (b) 0.25, and (c) 0.5 M.

SCHEME 1: Schematic Representations of P123 and CTAB and Their Assembly in the Presence of Sulfate Ion



the addition of CTAB to these solutions clears the solution by breaking down the P123 aggregates into micelles and/or to molecular species.

Since the sulfate ion decrease the solubility of P123 and increase the aggregation number in the micelle, one would expect a pore size expansion in the synthesized mesoporous silica particles. Table 1 summarizes the N_2 sorption data of the particles, obtained from the CTAB–P123– SO_4^{2-} system. The general trend is an increase in pore size and pore volume and a decrease in the surface area with an increasing SO_4^{2-} ion concentration; see Figure 4 and Table 1. Since the amount of silica source is the same in all preparations and the aggregation number increases with an increasing SO_4^{2-} ion concentration, the number of micelles in the solution decreases, and as a result the excess silica formed a significant amount of nonporous silica, which correlates well with the measured low surface area. Notice also that the wall thickness (t), which can be defined as the sum of the shell thickness of adjacent micelles and the distance between them also decreases with an increasing SO_4^{2-} concentration; see illustration in Scheme 1. This is also consistent with the fact that the shell thickness of the micelle decreases with an increasing aggregation number.⁴⁷

The excess silica in the media may also create nonporous or microporous plugs^{48–50} that settle in the pore structure and show a pore blocking effect in the mesoporous particles. The plugging

of the pores can be observed in the N_2 adsorption–desorption isotherms. Figure 4 shows the N_2 sorption isotherms of the mesoporous particles obtained from the CTAB–P123– SO_4^{2-} system. The changes in the pore volume of the samples with increasing SO_4^{2-} ion also correlate this conclusion, see Table 1. At low CTAB concentrations (where the CTAB/P123 mol ratio is 3.0) and in the presence of SO_4^{2-} ions, a very sharp step is observed in desorption branch of the isotherm. When the CTAB concentration is increased (CTAB/P123 mol ratio of 4.0), the plugging gets smaller, which can also be understood from the desorption branch. The step originating from the plugs gets smoother since there are more CTAB molecules to form more CTAB–P123 micelles. When the CTAB/P123 mol ratio is 6.0, no plug formation is observed (desorption branch displays type II hysteresis loop); however, the pore structure becomes an ink-bottle type. That means the pore structure is not cylindrical anymore and it has wide and narrow sections.

The Effect of Nitrate Ion in the CTAB–P123– NO_3^- Synthesis System. The NO_3^- ion has no significant effect on the micellization of the pluronic surfactants; see Supporting Information Figure S1. In this investigation, we have used the NO_3^- ion because in the presence of a more hydrotropic anion the CTAB is insoluble, such that it increases the amount of CTAB in the CTAB–P123 micelles (see later). Upon using the nitrate salt in our reaction media, we have observed that the CTAB content of the micelles increases. The amount of CTA^+ in the micelle is a function of both the concentration of CTAB and NO_3^- ion. Increasing the amounts of CTAB in the micelle results in a size decrease of the micelle and a unit cell decrease in the silica particles. At a CTAB/P123 mol ratio of 3.0 and 0.50 M NO_3^- , the position of the first diffraction line, (100), shifts to higher angles indicating a decrease in the unit cell (from 8.8 to 8.1 nm). The PXRD pattern still shows an ordered 2D hexagonal mesostructure; see Figure 5A. The (110) and (200) planes are also well resolved in this composition. However the unit cell size decreases about 9% and the surface area drops about 42% (from 690 to 399 m^2/g), see Table 2. A further increase of the nitrate ion concentration to 1.0 M does not change the position of the (100) line; however, the intensity is drastically decreased. In addition, the diffraction lines due to (110) and (200) planes are not visible, indicating a disordered mesostructure. At a CTAB/P123 mol ratio of 6.0, the position of the first diffraction line (100) further shifts to higher angles, corresponding to a 22% shrinkage (unit cell changes from 8.4 to 6.5 nm) at both nitrate concentrations, compared to the nitrate free case, Figure 5B. The surface area drop is about 23% at 0.5 M (from 723 to 555 m^2/g) and 16% at 1.0 M nitrate concentration (from 723 to 609 m^2/g). The silica particles are still ordered and three diffraction lines are intense enough to index to (100),

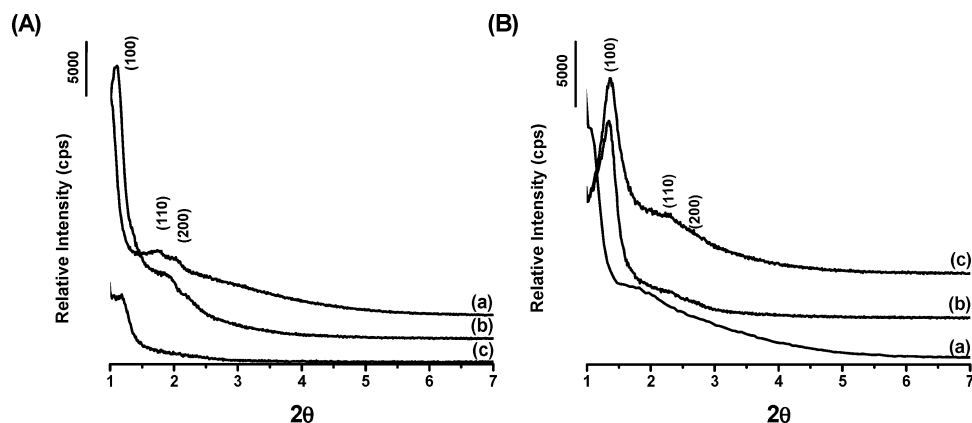


Figure 5. The PXR D patterns of the mesostructured silica obtained from the CTAB–P123–NO₃[−] system at different NO₃[−] ion concentrations and CTAB/P123 mol ratios. (A) The CTAB/P123 mol ratio of 3.0 and the nitrate ion concentration of (a) 0.0, (b) 0.5, and (c) 1.0 M. (B) The CTAB/P123 mol ratio of 6.0 and the nitrate ion concentration of (a) 0.0, (b) 0.5, and (c) 1.0 M.

SCHEME 2: Schematic Representation of CTAB/P123 in the Presence of Nitrate Ion

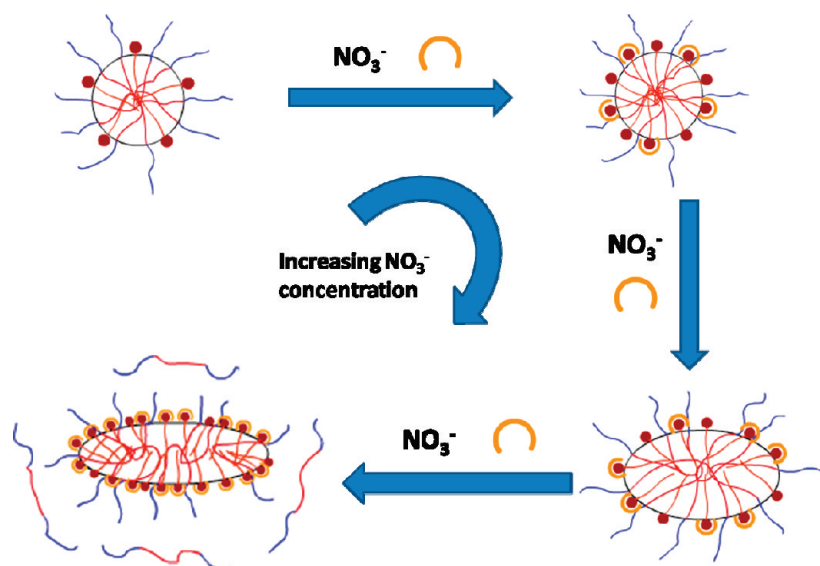


TABLE 2: The Structural Parameters of the CTAB–P123–NO₃[−] System in Different CTAB/P123 Mol Ratios and NO₃[−] Ion Concentrations

CTAB/P123 mol ratio	NaNO ₃ concentration (M)	BET surface area (m ² /g)	<i>d</i> ₁₀₀ (nm)	pore size ^a 2 <i>r</i> (nm)	wall thickness ^b (nm)	pore volume (cm ³ /g)
3	0	690	8.8	5.9	4.3	0.40
	0.50	399	8.1	5.9	3.8	0.47
	1.00	112	7.5	5.6	3.1	0.21
6	0	723	8.4	4.6	4.7	0.54
	0.50	555	6.5	4.5	3.0	0.46
	1.00	609	6.5	4.2	3.2	0.60

^a Pore diameter is calculated from the adsorption branch of the isotherm by BJH method. ^b The wall thickness *t* is obtained by deducing the pore diameter (2*r*) from the unit cell *a*₀ (*a*₀ = (2/√3)*d*₁₀₀), namely, *t* = *a*₀ − 2*r*.

(110), and (200) planes of the 2D hexagonal mesostructure at 6.0 CTAB/P123 mol ratio.

At low CTAB concentrations (CTAB/P123 mol ratio of 3.0) and in the presence of a nitrate ion in the media, the CTAB ratio in the CATB/P123 micelles is increased, which means there is always free P123 molecules or species in the media; see Scheme 2. These species assemble with the silica species to form nonporous or microporous domains in/on the particles. Therefore, the meso-order in the particles decreases, especially at high nitrate concentrations (1.0 M and above). The nonporous or microporous particles also cause a sharp decrease in the surface area; see Table 2. However in the presence of excess

CTAB in the reaction media (CTAB/P123 mol ratio of 6.0), there is always enough CTAB to maintain the cooperative micellization, therefore highly ordered particles are formed with a smaller unit cell and an increased surface area due to increased CTAB/P123 ratio in the micelles.

Mainly spherical particles are formed at low NO₃[−] ion concentrations (0.5 M) and wormlike particles at high NO₃[−] ion concentrations (1.0 M). This means that the nitrate ion does not affect the P123 domains, but it decreases the CTAB solubility. The NO₃[−] anion probably causes the formation of the micelles with an excessive amount of CTA⁺ together with nitrate anions. Moreover, the TEM images also correlate with

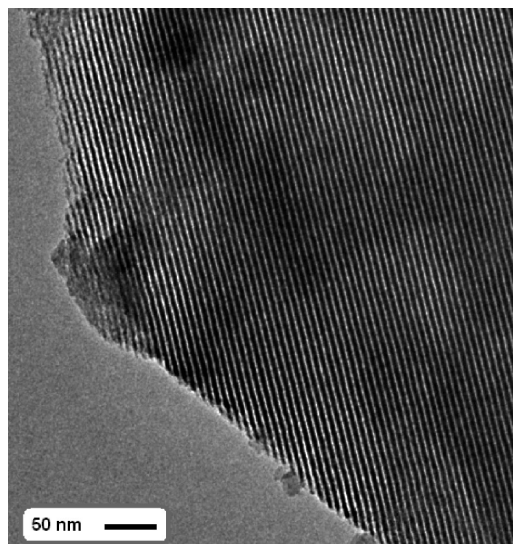


Figure 6. The TEM images of the mesoporous silica particle obtained from the CTAB–P123–NO₃[−] system with a CTAB/P123 mol ratio of 6.0 and the NO₃[−] ion concentration of 1.0 M. Scale bar is 50 nm.

the formation of a highly ordered pore structure in the presence of excess CTAB and NO₃[−] anion, Figure 6. The TEM image shows a long-range order with a repeating distance of 6.6 nm, which is consistent with the calculated *d*-spacing from the PXRD patterns.

The amount of CTAB in the mesostructured particles upon addition of nitrate salt can also be determined using FTIR and Raman spectroscopy (Figure 7). At low CTAB concentrations (CTAB/P123 mol ratio of 3.0), the spectrum does not show any difference until the NO₃[−] ion concentration reached 1.0 M in which the as-synthesized silica particles contain excessive amount of CTANO₃; see Figure 7A. The progression of *ν*-CH symmetric and asymmetric stretching modes of the alkyl chains, which are observed at 2850 and 2885 cm^{−1}, respectively, can be monitored. The low intensity of the P123 related signals in the FTIR spectra indicates that at high NO₃[−] ion concentrations, some of the P123 molecules are solvated out from the micelle, as free surfactants in the solution. The free P123 molecules assemble together with some of the silica species in the media and form a significant amount of nonporous silica. However, in the presence of enough CTAB in the media (such as in the case of a CTAB/P123 mol ratio of 6.0), most of the P123 molecules are incorporated into the micelles, where the intensity of the P123 signals do not change, but the CTAB signals increase with an increasing NO₃[−] ion in the media; see Figure 7B,C. As a result, the silica particles have a higher surface area, Table 2. Notice also that the particles have a larger surface area and smaller wall thickness in the CTAB only systems however the particles synthesized using P123 have a smaller surface area and thicker walls, which correlate with our observations and conclusions.

The role of the NO₃[−] ions in the assembly process is very important because one can control the amount of CTAB molecules in mesostructured particles using nitrate ion in the synthesis media, and as a result the pore size and wall-thickness in the particles. Also note that under our synthesis conditions, it is not possible to synthesize mesoporous particles without P123. In the absence of P123 and a nitrate ion, the reaction results in a gel that dries into a completely disordered white powder. However, it is possible to synthesize mesoporous particles using CTAB–NO₃[−] couple at a lower nitrate ion concentration, see Supporting Information Figure S2.

The Effect of the Chloride Ion on the CTAB–P123–Cl[−] Synthesis System. In the Hofmeister series, the Cl[−] anion is in between the SO₄^{2−} and NO₃[−] ions and its effect is also in between SO₄^{2−} and NO₃[−] ions, in terms of the assembly of both P123 and CTAB. It affects the aggregation of these two surfactants by decreasing the solubility of both P123 and CTAB. However, it is not as effective as SO₄^{2−} for decreasing the solubility of P123 or NO₃[−] ion for decreasing the solubility of the CTAB. Figure 8 shows the PXRD patterns of the calcined samples, obtained from the CTAB–P123–Cl[−] systems. In the presence of a 3.0 CTAB/P123 mol ratio and a 0.5 M chloride ion, the diffraction pattern shows three distinct diffraction lines, which can be indexed to (100), (110), and (200) planes of 2D hexagonal structure. When compared to the chloride-free system, the diffraction lines shift to higher angles (from 1.0 to 1.2°, 2θ) and the unit cell decreases from 10.2 to 8.5 nm; see Table 3. Increasing the Cl[−] ion concentration to 1.0 M causes a further shift of the diffraction lines and the unit cell parameter decreases to 8.0 nm. However, the (110) and (200) diffraction lines are not well resolved and appear together as a broad peak, indicating a decrease in the order of the channels in the particles. On the other hand, at a high CTAB/P123 mol ratio (6.0), the existence of the chloride ion causes a decrease in the meso-order. Besides decreasing the intensity of the first diffraction line (100), the (110) and (200) diffraction lines disappear.

At low CTAB/P123 mol ratios, the effect of the Cl[−] ion is very similar to that of SO₄^{2−} ion. The main effect at low concentrations is on the P123, however it is mainly on the CTAB at higher Cl[−] ion concentrations (1.0 M). The effect of the Cl[−] ion on the CTAB increases with an increasing amount of CTAB in the media. Therefore, the Cl[−] ion in the CTAB–P123–Cl[−] system is more effective at lower Cl[−] ion concentrations in the presence of higher CTAB/P123 mol ratios. The changes in the structural parameters, in the CTAB–P123–Cl[−] system, are a result of a combination of the effects of the SO₄^{2−} and NO₃[−] ions, see Table 3. The Cl[−] ion is not as effective as NO₃[−] in terms of decreasing the solubility of the CTAB and its effect on the P123 helps the CTAB molecules to stay in the micelle. To summarize, at low CTAB concentrations, the effect of the Cl[−] ion is mainly in favor of decreasing the solubility of P123, but at high CTAB concentrations, it is mainly on the CTAB. The Cl[−] ion increases the CTAB/P123 mol ratio in the micelles. This results in a decrease in the pore order and pore size distributions of the particles; see Table 3.

The Cl[−] ion has no effect on the morphology at low CTAB and Cl[−] ion concentrations (Supporting Information Figure S3). The samples contain a mixture of spherical and wormlike particles at all CTAB and Cl[−] ion concentrations. In addition, these particles are highly ordered and mesoporous; see the TEM images in Supporting Information Figure S3. Further increasing the Cl[−] anion concentration starts to influence the CTAB molecules, where no distinct morphology was obtained. Notice also that a similar effect is observed in the surface area and diffraction characteristic of these particles. At 0.5 M chloride, the particles are spherical but their surfaces are cornered. When the concentration is increased to 1.0 M, the particles are perfectly spherical with some crystalline features on the surface of these particles. A careful EDS analysis of these crystalline features shows that they are silica species.

As in the case of nitrate, the amount of the Cl[−] ion also increases the number of CTAB in the CTAB/P123 micelles, which can be determined using FTIR spectroscopy; Supporting Information Figure S4. Different from the NO₃[−] ion, the Cl[−] ion becomes effective in increasing the amount of CTAB in

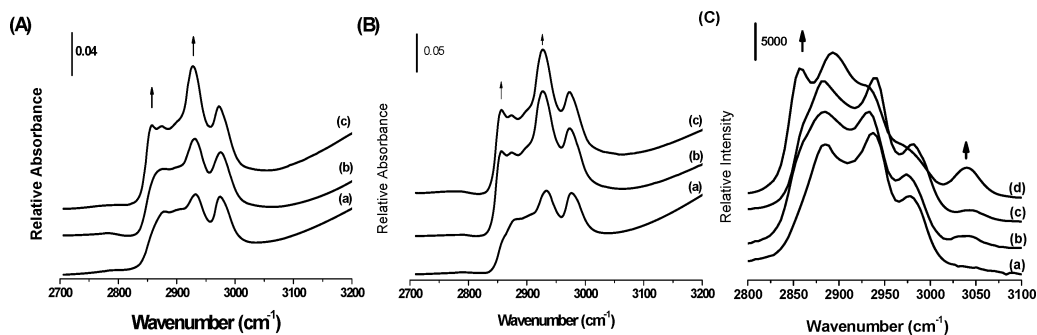


Figure 7. The FTIR spectra of the mesostructured silica particles obtained from the CTAB–P123–NO₃[−] system with different NO₃[−] ion concentrations and CTAB/P123 mol ratios. (A) The CTAB/P123 mol ratio of 3.0 and the nitrate ion concentration of (a) 0.0, (b) 0.5, and (c) 1.0 M. (B) The CTAB/P123 mol ratio of 6.0, and the nitrate ion concentration of (a) 0.0, (b) 0.5, and (c) 1.0 M. (C) The Raman spectra of the mesostructured silica particles obtained from the CTAB–P123–NO₃[−] system with a CTAB/P123 mol ratio of 6.0 and the NO₃[−] ion concentrations of (a) 0.0, (b) 0.5, and (c) 1.0, and (d) the CTAB–NO₃[−] system.

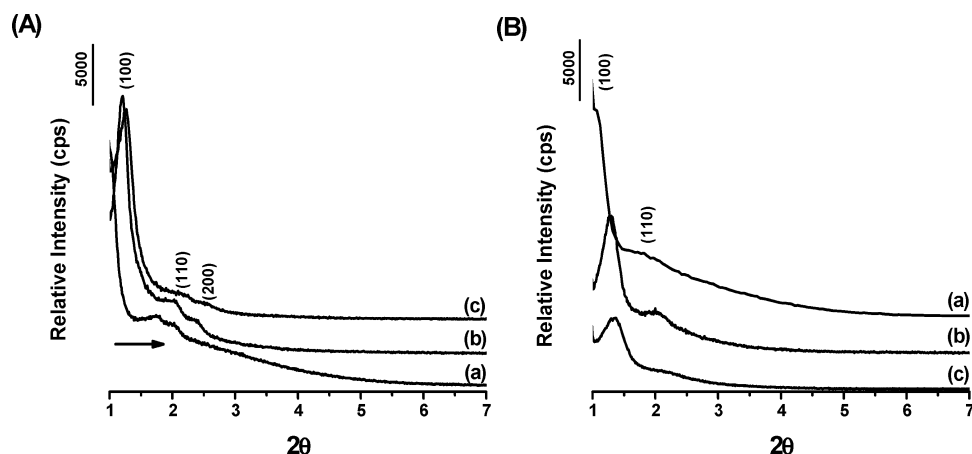


Figure 8. The PXRD patterns of the mesostructured silica obtained from the CTAB–P123–Cl[−] system at different Cl[−] concentrations and CTAB/P123 mol ratios. (A) The CTAB/P123 mol ratio of 3.0 and the chloride ion concentration of (a) 0.0, (b) 0.5, and (c) 1.0 M. (B) The CTAB/P123 mol ratio of 6.0 and the chloride ion concentration of (a) 0.0, (b) 0.5, and (c) 1.0 M.

TABLE 3: The Structural Parameters of the CTAB–P123–Cl[−] System in Different CTAB/P123 Mol Ratios and Cl[−] Concentrations

CTAB/P123 mol ratio	NaCl Concentration (M)	BET surface area (m ² /g)	<i>d</i> ₁₀₀ (nm)	pore size ^a 2 <i>r</i> (nm)	wall thickness ^b (nm)	pore volume (cm ³ /g)
3	0	690	8.8	5.9	4.3	0.40
	0.50	454	7.4	4.5	4.0	0.41
	1.00	196	6.9	4.2	3.8	0.26
6	0	723	8.4	4.6	4.7	0.54
	0.50	354	6.8	4.8	3.0	0.53
	1.00	185	6.5	4.9	2.6	0.25

^a Pore diameter is calculated from the adsorption branch of the isotherm by BJH method. ^b The wall thickness *t* is obtained by deducing the pore diameter (2*r*) from the unit cell *a*₀ (*a*₀ = (2/√3)*d*₁₀₀), namely, *t* = *a*₀ − 2*r*.

the mesostructured particles at the higher Cl[−] concentrations (1.0 M) and low CTAB/P123 mol ratios. The effect of the Cl[−] ion at high CTAB/P123 mol ratios (6.0) is very similar to the NO₃[−] ions. The symmetric *ν*-CH stretching peak at 2850 cm^{−1} in the FTIR spectrum and 2846 cm^{−1} in the Raman spectrum of the methylene groups appear as a shoulder and increases in intensity together with the other signals of CTAB with increasing Cl[−] ion concentration.

If there is enough CTAB in the reaction media, all particles show a type IV isotherm, which is characteristic for mesoporous materials; see Figure 9. When the Cl[−] ion concentration reaches 1.0 M, it starts to affect the CTAB solubility, where the micelle starts to take more CTAB molecules. Increasing the amount of CTAB decomposes the micelles, where more disordered particles are formed. Moreover, the N₂ desorption curves of these

particles show a type II hysteresis loop, which means the pore structure is ink-bottle type; see Figure 9. As a summary, at a low CTAB/P123 mol ratio (3.0) and low Cl[−] ion concentration (0.5 M), the particles have cylindrical pores but pore blocking is observed at high Cl[−] ion concentration (Figure 9A). At high CTAB/P123 mol ratio (6.0), the pores are ink-bottle type (Figure 9B). These are also consistent with the changes in the pore volumes; see Table 3.

The Effect of Benzene in the CTAB–P123–benzene Synthesis System. The benzene molecule is almost insoluble in water but soluble to some extent in the aqueous P123 solution. When the benzene molecules penetrate the core of the CTAB/P123 micelles, they dry the core and enlarge the micelles. As stated before in the CTAB–P123–SO₄^{2−} system, a dehydrated core means more ordered particles. In the CTAB–P123–SO₄^{2−}

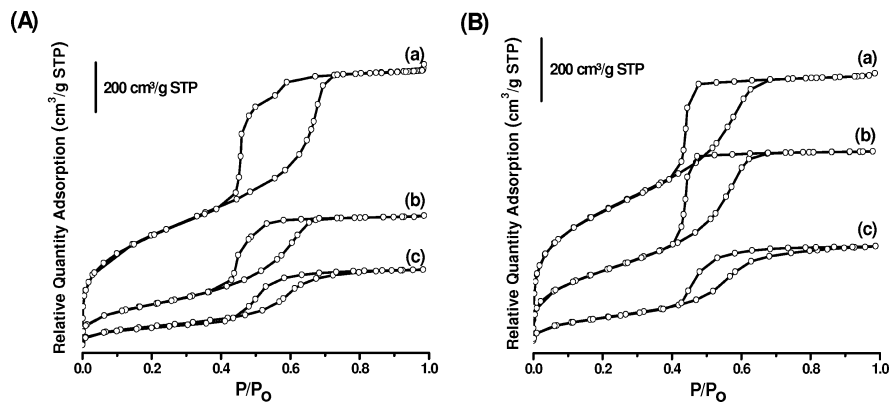


Figure 9. The N_2 adsorption–desorption isotherm of the mesoporous silica particles obtained from the CTAB–P123– Cl^- system. (A) For the CTAB/P123 mol ratio of 3.0 and the Cl^- ion concentrations of (a) 0.0, (b) 0.5, and (c) 1.0 M and (B) for the CTAB/P123 mol ratio of 6.0 and the Cl^- ion concentration of (a) 0.0, (b) 0.5, and (c) 1.0 M.

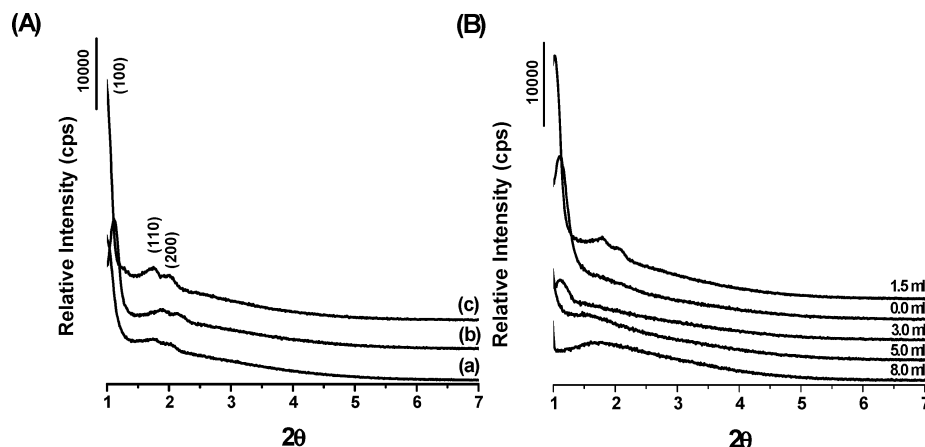
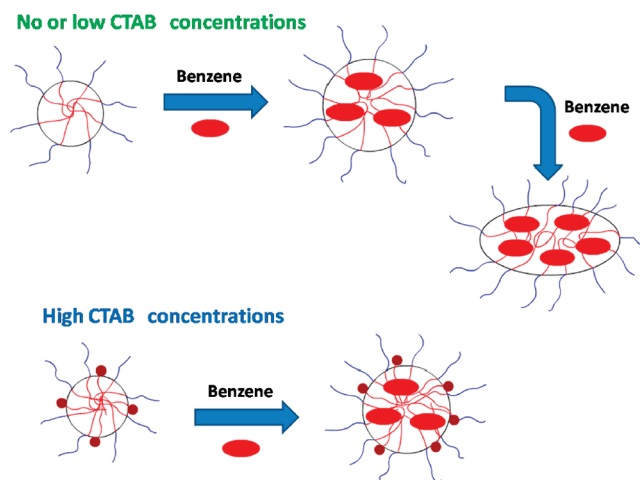


Figure 10. The PXRD patterns of the mesostructured silica particles obtained from the CTAB–P123–benzene systems at different benzene concentrations and CTAB/P123 mol ratios. (A) The CTAB/P123 mol ratio of 3.0 and benzene concentration of (a) 0.0, (b) 1.1×10^{-3} and (c) 3.4×10^{-3} M. (B) The CTAB/P123 mol ratio of 6.0 and benzene concentration as indicated in the graphs.

system, a dehydrated core has been achieved by increasing the micelle aggregation number; however in the CTAB–P123–benzene system, a dry core is achieved by adding benzene into the core of the micelle. Figure 10 shows the PXRD patterns of the as-synthesized particles using the CTAB–P123–benzene system. At low CTAB/P123 mol ratios (3.0), the benzene molecules form more ordered particles than at higher CTAB/P123 mol ratios (6.0). Besides the (100) plane, the other higher order diffraction lines ((110) and (200)) also have higher intensities and are well resolved at a 3.0 mol ratio (CTAB/P123, Figure 10A). At a 4.0 mol ratio (CTAB/P123), the samples show an intermediate behavior between 3.0 and 6.0 mol ratios. This phenomenon can be explained by looking at the role of the CTAB in the assembly of pluronic surfactants. With CTAB free or low CTAB concentrations, an increase in the hydrophobic character of the micelle results in a geometry change from spherical micelle to elongated micelle, see illustration in Scheme 3. However, at high CTAB concentrations, the geometry change was suppressed by the positively charged headgroup repulsions. The positively charged headgroup of the CTAB is accommodated in the core–corona interface, where the effective headgroup area is highest in a spherical packing. Therefore, a higher CTAB content in the micelle forces the surfactants to pack in a spherical geometry.

Interestingly the benzene solubility is independent of the amount of CTAB but the existence of CTAB changes the order and morphology of the particles. The benzene solubility limit in the CTAB–P123–benzene system only depends on the amount of P123.

SCHEME 3: Schematic Representation of the CTAB/P123 Assembly in the Presence of Benzene



In our synthesis conditions, the maximum amount of benzene that forms a clear solution at RT is around 5 mL (5.65×10^{-3} M) in a 100 mL aqueous solution. Increasing the amount of benzene further results a slurry solution that can be used further by adding TMOS; the resulting materials are still highly mesoporous but poorly ordered (see Table 4). This amount of benzene (5.65×10^{-3} M) might be still soluble since at higher temperatures the hydrophobicity of P123 micelles and the solubility capacity of the hydrophobic core increase. A clear

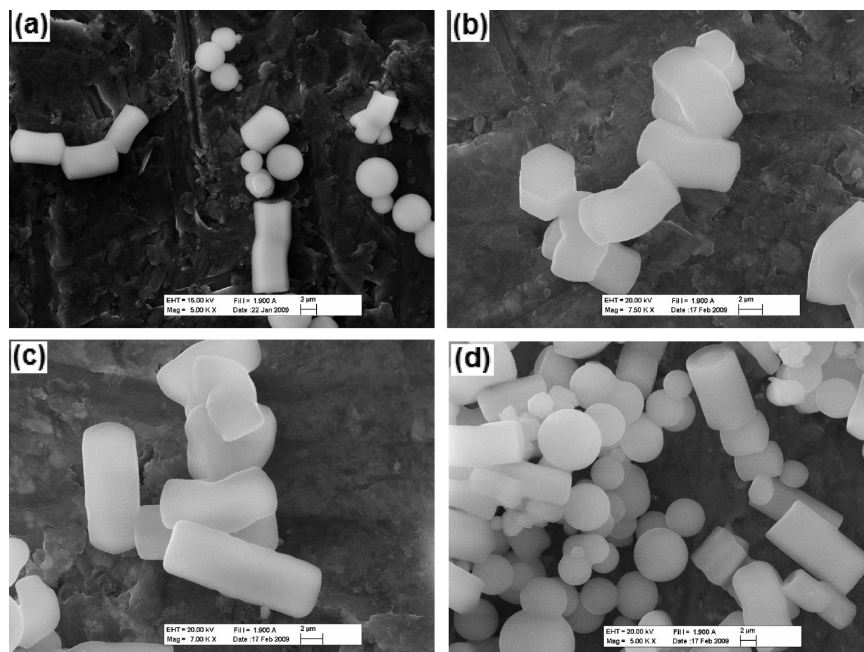


Figure 11. The SEM images of the particles synthesized using the CTAB-P123-benzene system for the CTAB/P123 mol ratio of 3.0 and the benzene concentration of (a) 0.0, (b) 1.1×10^{-3} , (c) 2.3×10^{-3} , and (d) 3.4×10^{-3} M.

TABLE 4: The Structural Parameters of the CTAB-P123-benzene System at Different CTAB/P123 Mol Ratios and Benzene Concentration

CTAB/P123 mol ratio	benzene ($\times 10^{-3}$ M)	BET surface area (m^2/g)	d_{100} (nm)	pore size ^a $2r$ (nm)	wall thickness t^b (nm)	pore volume (cm^3/g)
3	0	690	8.8	5.9	4.3	0.40
	1.13	665	7.9	5.5	3.7	0.60
	2.26	756	7.9	5.7	3.5	0.65
	3.39	696	8.8	6.6	3.5	0.74
4	0	685	7.9	4.1	5.0	0.34
	1.70	687	7.9	5.4	3.7	0.78
	3.39	645	7.9	5.4	3.7	0.67
	5.65	690		6.9		0.55
6	9.04	717		6.7		0.66
	0	723	8.4	4.6	4.7	0.54
	1.13	619	8.1	4.7	4.6	0.43
	2.26	665	8.5	4.9	4.8	0.50
	3.39	643	8.9	5.6	4.7	0.58

^a Pore diameter is calculated from the adsorption branch of the isotherm by BJH method. ^b The wall thickness, t is obtained by deducing the pore diameter ($2r$) from the unit cell a_0 ($a_0 = (2/\sqrt{3})d_{100}$), namely, $t = a_0 - 2r$.

solution might be obtained at higher temperatures (further steps of the reaction). However, even at higher temperatures benzene has a solubility limit. The highest amount of benzene that can be used to obtain mesoporous materials is about 8 mL (9.04×10^{-3} M). Above these concentrations, the particles are disordered and no distinct morphology was obtained (not shown).

The effect of benzene on the morphology can be classified in three groups in terms of the CTAB/P123 mol ratio. The first group is the low CTAB/P123 mol ratios (3.0 and below), the second is the high CTAB/P123 mol ratios (6.0 and higher), and the last group contains the intermediate concentrations. At high CTAB/P123 mol ratios (6.0), the benzene has no observable effect on the morphology (not shown) and in the diffraction patterns. Figure 11 shows the SEM images of the samples obtained from the CTAB-P123-benzene system at low CTAB/P123 mol ratios (3.0). Notice that in the absence of benzene a mixture of spheres and wormlike particles are formed (Figure 10a). By increasing the concentration of benzene (to 1.1×10^{-3} M) all the particles are predominantly wormlike (Figure 11b,c). As discussed in the previous paragraphs, the meso-order also

increases in these elongated particles. A further increase in the amount of benzene not only increases the order of the particles but also some elongated crystalline particles are also observed (Figure 11b). A side view of the crystalline particles clearly shows that they are perfectly hexagonal (Figure 11c). Note also that these elongated particles are also birefringent under a polarized optical microscope indicating a 2D hexagonal mesostructure (not shown). Surprisingly, at 3.4×10^{-3} M and higher benzene concentrations, the number of spherical particles increases and a mixture of spherical and wormlike particles are obtained (Figure 11d). The most reliable explanation for this observation can be of the effect of benzene as a solvent (starts forming its own phase in the solution). When it is used in excess, it is no longer acting as an additive but it is a cosolvent. By taking into consideration that benzene is a much better solvent than water for pluronic surfactants, a decrease of the meso-order and morphology change is not a surprise.

The CTAB/P123 mol ratio of 4.0 can be considered as an intermediate concentration in the CTAB-P123-benzene system. At this mole ratio, the benzene molecules cause the

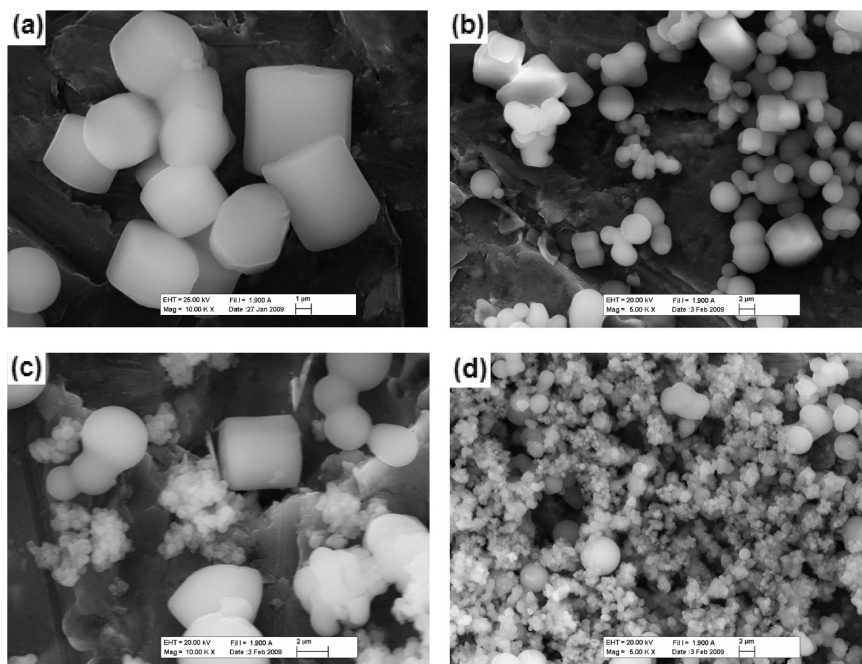


Figure 12. The SEM images of the samples, synthesized using the CTAB–P123–benzene system with a CTAB/P123 mol ratio of 4.0 and the benzene concentration of (a) 1.7×10^{-3} , (b) 3.4×10^{-3} , (c) 5.7×10^{-3} , and (d) 9.0×10^{-3} M.

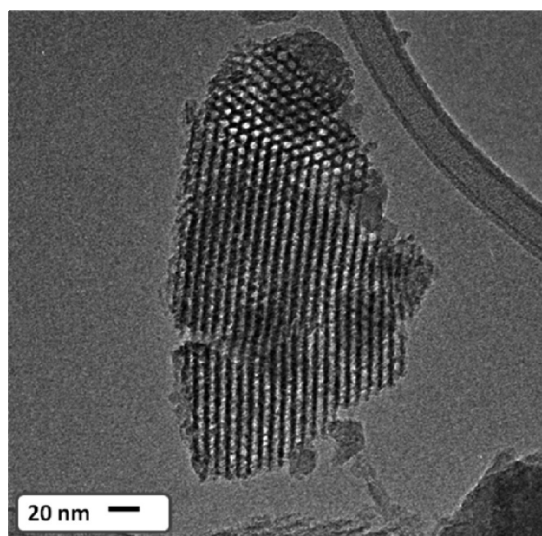


Figure 13. The TEM images of a sample obtained from the CTAB–P123–benzene system; the CTAB/P123 mol ratio of 4.0 and the benzene concentration of 1.7×10^{-3} M.

formation of various morphologies from the same synthesis pot (Figure 12). At 1.7×10^{-3} and 3.4×10^{-3} M concentrations, the observed morphologies are spherical, wormlike, crystal-like, coin type, gyroid, bagel, and gyroscope type. To the best of our knowledge, the gyroscope type particles have not been observed yet. In general, the particles at this CTAB/P123 mol ratio (4.0) are shorter in length and more oval when compared to the particles synthesized at 3.0 mol ratio in the CTAB–P123–benzene system. When the benzene concentration is above $\sim 5.0 \times 10^{-3}$ M, disordered particles start to form and the amount increase with an increasing benzene concentration; see Figure 12c,d. Note also that these particles are completely disordered.

The TEM images also support that highly ordered 2D hexagonal particles are formed from the CTAB–P123–benzene system, Figure 13. The top part of the TEM image in Figure 13 is a perfect illustration of hexagonal ordering. The pore channels of these particles are straight and continue through

the particle, Figure 13. The most characteristic property of the organic additives is their role as a pore swelling agent. Therefore, an increase in the pore size distribution is also observed in the samples of the CTAB–P123–benzene system, depending on the CTAB and benzene concentration; see Table 4. At low CTAB/P123 mol ratios (3.0 and 4.0), the wall thickness decreases with increasing benzene, which can be attributed to a decreased repulsion between the benzene-containing micelles or increased hydrophobic interaction in the micelles, Table 4. However no wall thickness changes but a pore size expansion is observed only at high benzene concentrations and high CTAB concentrations (CTAB/P123 mol ratios of 6.0).

Conclusions

The role of organic (benzene) and inorganic (salts) additives on the assembly of CTAB-P123 surfactant couple and the morphology of the mesoporous silica particles has been investigated. Three different Hofmeister anions, one lyotropic anion, SO_4^{2-} , one hydrotropic anion, NO_3^- , and one anion in between sulfate and nitrate ions, Cl^- , have been used to influence the CTAB-P123 assembly. The effect of the sulfate ion is mainly on the P123 component of the couple. It dehydrates the core of the CTAB-P123 micelles, increases the aggregation number (number of P123 molecules in the micelle increases), and as result increases the pore size while the wall decreases in thickness in the silica particles. The nitrate ion increases the number of CTAB in the CTAB-P123 micelles, and as a result one obtains silica particles with smaller unit cells. Therefore at low CTAB concentrations the CTAB is consumed in early stages of the reaction, the remaining excess P123 in the solution form nonporous or microporous species in/on the mesoporous silica particles, and as a result the surface area decreases with an increasing nitrate salt content of the reaction media. However, at higher CTAB concentrations, the effect is on the morphology of the particles. In general, increasing the amount of CTAB in the CTAB-P123 systems forces the formation of spherical particles; however in the presence of a nitrate ion in the media, wormlike particles form at higher CTAB concentrations. The

chloride ion is between the sulfate and nitrate ions in the Hofmeister series, and its effect on the properties of the silica particles is also between these two ions. Increasing Cl^- ion in the media decreases the solubility of both CTAB and P123 and causes a diminished unit cell and less order in the channel structure. The effect is mainly on the P123 at low CTAB/P123 mol ratios, but at high CTAB/P123 it affects both the CTAB and P123. The benzene molecule has effects similar to the sulfate ion, but the effect is predominantly on the core of the micelles, and as a result various morphologies with an expanded pore structure can be obtained.

The pore size, pore structure, and the morphology can be controlled by the additives in the synthesis of mesoporous silica particles using CTAB-P123 couple. The spherical, wormlike, ropelike, crystal-like, coin type, gyroid, bagel, and gyroscope type morphologies can be obtained from this system by carefully adjusting the CTAB/P123 mol ratio and the additive type and its concentration in the synthesis media. The pore size (between 3.4 and 7.0 nm) and pore structure (cylindrical, plugged, and ink-bottle) of the particles can also be adjusted by controlling the assembly of the CTAB/P123 couple during the synthesis.

Acknowledgment. We would like to thank Mr. Emre Tanır for the TEM measurements and to TÜBİTAK under a project 107T837, TÜBA (Turkish Academy of Science), and a European project, REGPOT-UNAM (Contract No. 203953) for the financial support. A.S.P. also thanks TÜBİTAK for a graduate student scholarship.

Supporting Information Available: Micellization plots, photographs, UV–vis absorption spectra, and more SEM, TEM, and FTIR data. This material is available free of charge via the Internet at <http://pubs.acs.org>.

References and Notes

- (1) Kresge, C. T.; Leonowicz, M. E.; Roth, W. J.; Vartuli, J. C.; Beck, J. S. *Nature* **1992**, *359*, 710.
- (2) Yanagisawa, T.; Shimizu, T.; Kuroda, K.; Kato, C. *Bull. Chem. Soc. Jpn.* **1990**, *63*, 988.
- (3) Yang, H.; Coombs, N.; Ozin, G. A. *Nature* **1997**, *386*, 692.
- (4) Mizutani, M.; Yamada, Y.; Yano, K. *Chem. Commun.* **2007**, 1172.
- (5) Mesa, M.; Sierra, L.; Patarin, J.; Guth, J. L. *Solid State Sci.* **2005**, *7*, 990.
- (6) Poyraz, A. S.; Albayrak, C.; Dag, Ö. *Microporous Mesoporous Mater.* **2008**, *115*, 548.
- (7) Yu, C. Z.; Tian, B. Z.; Fan, J.; Stucky, G. D.; Zhao, D. Y. *J. Am. Chem. Soc.* **2002**, *124*, 4556.
- (8) Chen, Q. R.; Sakamoto, Y.; Terasaki, O.; Che, S. A. *Microporous Mesoporous Mater.* **2007**, *105*, 24.
- (9) Leonard, A.; Blin, J. L.; Robert, M.; Jacobs, P. A.; Cheetham, A. K.; Su, B. L. *Langmuir* **2003**, *19*, 5484.
- (10) Chan, H. B. S.; Budd, P. M.; Naylor, T. D. *J. Mater. Chem.* **2001**, *11*, 951.
- (11) Wang, B.; Chi, C.; Shan, W.; Zhang, Y. H.; Ren, N.; Yang, W. L.; Tang, Y. *Angew. Chem., Int. Ed.* **2006**, *45*, 2088.
- (12) Prouzet, E.; Cot, F.; Boissiere, C.; Kooyman, P. J.; Larbot, A. *J. Mater. Chem.* **2002**, *12*, 1553.
- (13) Yano, K.; Fukushima, Y. *J. Mater. Chem.* **2003**, *13*, 2577.

- (14) Yamada, Y.; Nakamura, T.; Ishi, M.; Yano, K. *Langmuir* **2006**, *22*, 2444.
- (15) Stein, A. *Microporous Mesoporous Mater.* **2001**, *44*, 227.
- (16) Trewyn, B. G.; Giri, S.; Slowing, I. I.; Lin, V. S. Y. *Chem. Commun.* **2007**, 3236.
- (17) Nakashima, K.; Bahadur, P. *Adv. Colloid Interface Sci.* **2006**, *123*, 75.
- (18) Patel, K.; Bahadur, P.; Guo, C.; Ma, J. H.; Liu, H. Z.; Nakashima, K. *J. Dispersion Sci. Technol.* **2008**, *29*, 748.
- (19) Malmsten, M.; Lindman, B. *Macromolecules* **1992**, *25*, 5440.
- (20) Zhang, W. H.; Zhang, L.; Xiu, J. H.; Shen, Z. Q.; Li, Y.; Ying, P. L.; Li, C. *Microporous Mesoporous Mater.* **2006**, *89*, 179.
- (21) Wan, Y.; Shi, Y. F.; Zhao, D. Y. *Chem. Commun.* **2007**, 897.
- (22) Yu, C. Z.; Fan, J.; Tian, B. Z.; Zhao, D. Y. *Chem. Mater.* **2004**, *16*, 889.
- (23) Carale, T. R.; Pham, Q. T.; Blankschtein, D. *Langmuir* **1994**, *10*, 109.
- (24) Patel, K.; Bahadur, P.; Guo, C.; Ma, J. H.; Liu, H. Z.; Yamashita, Y.; Khanal, A.; Nakashima, K. *Eur. Poly. J.* **2007**, *43*, 1699.
- (25) Bharatiya, B.; Ghosh, G.; Bahadur, P.; Mata, J. *J. Dispersion Sci. Technol.* **2008**, *29*, 696.
- (26) Kleitz, F.; Solovyov, L. A.; Anilkumar, G. M.; Choi, S. H.; Ryoo, R. *Chem. Commun.* **2004**, 1536.
- (27) Trong, L. C. P.; Djabourov, M.; Ponton, A. *J. Colloid Interface Sci.* **2008**, *328*, 278.
- (28) Alexandridis, P.; Holzwarth, J. F.; Hatton, T. A. *Macromolecules* **1994**, *27*, 2414.
- (29) Bedrov, D.; Smith, G. D.; Yoon, J. Y. *Langmuir* **2007**, *23*, 12032.
- (30) Yang, L.; Alexandridis, P.; Steytler, D. C.; Kositzka, M. J.; Holzwarth, J. F. *Langmuir* **2000**, *16*, 8555.
- (31) Goldmints, I.; vonGottberg, F. K.; Smith, K. A.; Hatton, T. A. *Langmuir* **1997**, *13*, 3659.
- (32) Ma, J. H.; Guo, C.; Tang, Y. L.; Wang, J.; Zheng, L.; Liang, X. F.; Chen, S.; Liu, H. Z. *Langmuir* **2007**, *23*, 3075.
- (33) Leontidis, E. *Curr. Opin. Colloid Interface Sci.* **2002**, *7*, 81.
- (34) Jain, N. J.; George, A.; Bahadur, P. *Colloids Surf., A* **1999**, *157*, 275.
- (35) Kunz, W.; Henle, J.; Ninham, B. W. *Curr. Opin. Colloid Interface Sci.* **2004**, *9*, 19.
- (36) Dag, Ö.; Alayoğlu, S.; Uysal, I. *J. Phys. Chem. B* **2004**, *108*, 8439.
- (37) Albayrak, C.; Gülten, G.; Dag, Ö. *Langmuir* **2007**, *23*, 855.
- (38) Stevens, W. J. J.; Lebeau, K.; Mertens, M.; Van Tendeloo, G.; Cool, P.; Vansant, E. F. *J. Phys. Chem. B* **2006**, *110*, 9183.
- (39) Zhao, D.; Feng, J.; Huo, Q.; Melosh, N.; Fredrickson, G. H.; Chemalka, B. F.; Stucky, G. D. *Science* **1998**, *279*, 548.
- (40) Zhou, G. W.; Chen, Y. J.; Yang, J. H.; Yang, S. H. *J. Mater. Chem.* **2007**, *17*, 2839.
- (41) Zhou, X. F.; Qiao, S. Z.; Hao, N.; Wang, X. L.; Yu, C. Z.; Wang, L. Z.; Zhao, D. Y.; Lu, G. Q. *Chem. Mater.* **2007**, *19*, 1870.
- (42) Hanrahan, J. P.; Donovan, A.; Morris, M. A.; Holmes, J. D. *J. Mater. Chem.* **2007**, *17*, 3881.
- (43) Zhang, H.; Sun, J. M.; Ma, D.; Bao, X. H.; Klein-Hoffmann, A.; Weinberg, G.; Su, D. S.; Schlogl, R. *J. Am. Chem. Soc.* **2004**, *126*, 7440.
- (44) Nagarajan, R. *Colloids Surf., B* **1999**, *16*, 55.
- (45) Nagarajan, R. *Polym. Adv. Technol.* **2001**, *12*, 23.
- (46) Bagshaw, S. A.; Bruce, I. J. *Microporous Mesoporous Mater.* **2008**, *109*, 199.
- (47) Jain, N. J.; Aswal, V. K.; Goyal, P. S.; Bahadur, P. *Colloids Surf., A* **2000**, *173*, 85.
- (48) Van Der Voort, P.; Ravikovitch, P. I.; De Jong, K. P.; Benjelloun, M.; Van Bavel, E.; Janssen, A. H.; Neimark, A. V.; Weckhuysen, B. M.; Vansant, E. F. *J. Phys. Chem. B* **2002**, *106*, 5873.
- (49) Li, Y.; Xu, R.; Couderc, S.; Bloor, D. M.; Holzwarth, J. F.; Wyn-Jones, E. *Langmuir* **2001**, *17*, 5742.
- (50) Thommes, M.; Smarsly, B.; Groenewolt, M.; Ravikovitch, P. I.; Neimark, A. V. *Langmuir* **2006**, *22*, 756.